J. Indian Inst. Sci., Nov.–Dec. 2005, **85**, 403–418

Conformations of triethylphosphate: A reanalysis of the matrix isolation spectra

K. SANKARAN, V. VENKATESAN[1], K. SUNDARARAJAN AND K. S. VISWANATHAN
Materials Chemistry Division, Indira Gandhi Centre for Atomic Research, Kalpakkam 603 102, India.
email: vish@igcar.ernet.in

Received on July 15, 2005; Revised on September 27, 2005.

Abstract

The conformations of triethylphosphate (TEP) were studied using *ab initio* molecular orbital methods to reanalyse earlier matrix isolation infrared data. We located a number of minima of which the lowest was a conformer corresponding to a $G^{\pm}G^{\pm}G^{\pm}$(ttt) structure, where the notation in upper case refers to the orientation of the carbon atom attached to the alkoxy oxygen, while that in the lower case refers to the terminal carbon atom. As a result of this work, the conformations of TEP and its matrix isolation infrared spectra are well understood for the first time. Furthermore, this study has also thrown light on the factors determining conformational preferences in organic phosphates.

Keywords: Triethylphosphate, *ab initio*, matrix isolation, infrared spectroscopy, conformations.

1. Introduction

The conformational analyses of molecules containing O–P–O segments play an important role in the structures of biologically important molecules, such as organic phosphates. However, only recently have the structure and spectroscopy of even the first member of the series of organic phosphates, trimethylphosphate (TMP), been reasonably well understood [1–4]. Triethylphosphate (TEP), with a longer alkyl chain than TMP, is expected to present a more complex conformational picture. In earlier studies on TEP from this laboratory, the vibrational features of the ground and excited state conformers were identified using matrix isolation experiments coupled with both effusive and supersonic sources [5, 6]. The assignments of the vibrational features in that work were made based on an earlier infrared work of Mortimer [7]. However, the structural details of the different conformers of TEP corresponding to the ground and excited states, computed using the AM1 hamiltonian, were in question at that time. In that study [5], we referred to the conformers as *G* and *H* to denote the ground and higher energy conformers, respectively. We had, however, admitted then, that while the structures computed using the AM1 method may be acceptable, the energy ordering of the various conformers provided by the AM1 method cannot be considered conclusive. This observation had been made based on our studies on TMP, where the struc-

*Author for correspondence.
[1]Present address: Department of Applied Chemistry & Institute of Molecular Science, National Chiao Tung University, 1001, Ta-Hsueh Rd., Hsinchu 30010, Taiwan

tures of TMP calculated using the AM1 hamiltonian and *ab intio* computations, at the HF and MP2 levels using a 6-31G** basis, were reasonably similar but not so the energy ordering of the conformers. It turned out then that only the results obtained through *ab initio* computations explained our matrix isolation experiments. In this study, we have reanalyzed the matrix isolation infrared spectra of our earlier work [5] and resolved the structural details of the conformers of TEP using *ab initio* method computations.

Given that the conformational picture of the TEP is complex, we believed that a search of the potential surface for the various conformers would be facilitated, if the factors determining conformational preferences in this molecule were first understood. Towards this end, we undertook a study of acetals and ketals, as these molecules have a backbone structure (C–O–C–O–C) similar to that found in organic phosphates (C–O–P–O–C).

Our work on acyclic acetals and ketals [8–11] showed that the anomeric carbon [12] in these systems adopted a *gauche* orientation. For example, in dimethoxymethane (DMM), the ground state conformer had a $G^{\pm}G^{m}$ structure, where G^{+} and G^{-} refer to the *gauche* orientation of the anomeric carbons [8]. Similar observations were made in other related systems, such as 1,1-dimethoxyethane (DME) [9] and 2,2-dimethoxypropane (DMP) [10]. These were useful lessons learnt from these studies regarding the influence of stereoelectronic effects, which we could transfer to our investigations on organic phosphates. For example, these conclusions helped in providing directions for rationalizing the conformations of TMP [2], where the lowest energy conformer was found to be one with a GGG structure (notations correspond to the O=P–O–C dihedrals), of C_3 symmetry. It seems likely that the orientation in this conformer was prompted by a combination of anomeric ($n–s^*$) and $n–p^*$ interactions in this molecule. Understanding the relative contributions of the two interactions in deciding conformational preferences in this molecule forms part of ongoing studies in this laboratory. The next higher energy conformer in TMP was a $G^{\pm}G^{\pm}T$ conformer (C_1 symmetry), followed by a $G^{+}G^{-}T$ geometry (C_s symmetry). At the B3LYP/6-31G** level, the first higher energy $G^{\pm}G^{\pm}T$ conformer was located 0.89 kcal/mol above the ground state conformer.

When we move from DMM to diethoxymethane (DEM) [11], we found that while the anomeric carbon continues to prefer a *gauche* orientation, the stability of the terminal carbon atom [13] in the C–C–O bond in DEM is decided by steric effects and hence adopts a *trans* orientation. Consequently, the $G^{\pm}G^{m}$(tt) is the ground state conformer, where the upper case refers to the orientation of the anomeric carbon and the lower case to that of the terminal carbon. It was also noted that the energy of the conformers increased as the terminal carbon atoms in the ground state $G^{\pm}G^{m}$(tt) conformer of DEM were progressively converted to *gauche* orientations. Consequently, the next higher energy conformer had a $G^{\pm}G^{m}$ ($g^{+}t$) structure.

The conclusions drawn from our studies on acetals and ketals were used in the study of the conformations of TEP. We predicted that the most stable geometry for TEP would be one where the anomeric carbons would adopt a *gauche* orientation, while the terminal carbons would take up a *trans* orientation; i.e. a $G^{\pm}G^{\pm}G^{\pm}$ (ttt) structure (where, once again, the upper case refers to the orientation of the anomeric carbon and the lower case to that of the terminal carbon). Higher energy conformers arise as the orientation of the anomeric carbons

was progressively converted to *trans* from their preferred *gauche* orientation. Likewise, the energies of the conformers are also likely to rise as the terminal carbons were converted to *gauche* from their preferred *trans* orientation. This predictive scheme greatly simplified our search for the conformers, as this study will show. Such predictive schemes, it may be emphasized, lead to a logical and systematic search for minima in such complex systems, as otherwise, a brute-force search of the potential surface is likely to be tedious and demanding on time and computer resources.

2. Computational methods

Ab initio molecular orbital calculations were performed using the Gaussian 98W program [14] on an Intel Pentium 4, 2.4 GHz machine. Geometry optimizations were done at the HF and B3LYP levels with analytical gradients using a 6-31G** basis set. All geometric parameters were optimized, and no constraints were imposed on the molecular geometry during the optimization process. Vibrational frequencies were computed for each of the structures to verify that they indeed corresponded to a minimum on the potential surface. The frequency calculations also helped in assigning the vibrational features of TEP obtained using matrix isolation infrared spectroscopic experiments. Only the computational results at the B3LYP/6-31G** level will be discussed here, as it best explains the experimental results from our earlier work.

3. Results and discussion

3.1. *Molecular geometry*

Based on the conformational picture of TMP, where the conformers were found to have $G^{\pm}G^{\pm}G^{\pm}$, $G^{\pm}G^{\pm}T$ and $G^{+}G^{-}T$ symmetries, the following general scheme of conformers may be written for TEP: $G^{\pm}G^{\pm}G^{\pm}$(xyz), $G^{\pm}G^{\pm}T$(xyz) and $G^{+}G^{-}T$(xyz). For example, the cluster of conformers for TEP that arises from the $G^{\pm}G^{\pm}G^{\pm}$ structure of TMP can be generated by running through all possible combinations of g^{+}, g^{-} and t, for the terminal carbon. One would then generate structures with orientations such as $G^{\pm}G^{\pm}G^{\pm}$(ttt), $G^{\pm}G^{\pm}G^{\pm}(g^{\pm}tt)$, $G^{\pm}G^{\pm}G^{\pm}(g^{m}tt)$, etc.

As discussed earlier, the ground state conformer of TEP would be expected to be $G^{\pm}G^{\pm}G^{\pm}$(ttt). One would also expect an increase in the energy of the conformers as we progressively move from $G^{\pm}G^{\pm}G^{\pm}$(ttt) to $G^{\pm}G^{\pm}G^{\pm}$(ggg) in TEP. The same picture is also expected to hold for the $G^{\pm}G^{\pm}T$(xyz) and $G^{+}G^{-}T$(xyz) structures.

Since the $G^{+}G^{-}T$ conformer has been computed to contribute to only a few per cent of the total population in TMP [4], we do not expect the structures of TEP that correlate with this structure of TMP to be of significance in assigning the spectra of TEP. We therefore studied only the cluster of conformers corresponding to $G^{\pm}G^{\pm}G^{\pm}$(xyz) and $G^{\pm}G^{\pm}T$(xyz) structures.

Ab initio computations were carried out to arrive at the conformations of TEP. We first performed geometry optimizations at the HF level using a 6–31G** basis set. Using these geometries, we then performed the computations at the B3LYP/6–31G** level (Fig. 1).

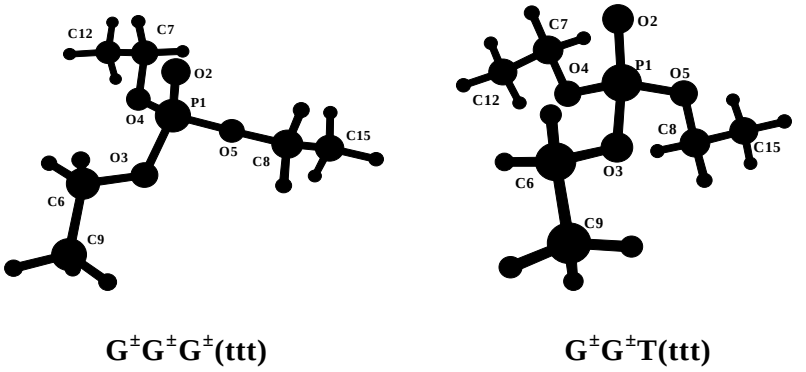

FIG. 1. Structures of TEP corresponding to the $G^{\pm}G^{\pm}G^{\pm}$(ttt) and $G^{\pm}G^{\pm}T$(ttt) conformers calculated at the B3LYP/6–31G** level.

Computationally, ten minima were identified corresponding to a cluster of conformers that arise from the $G^{\pm}G^{\pm}G^{\pm}$of TMP and 25 minima correlating with the $G^{\pm}G^{\pm}T$ structure of TMP. The relative energies of all the conformers at the B3LYP/6–31G** level, corrected for zero-point energies, are shown in Table I. The $G^{\pm}G^{\pm}G^{\pm}$ (ttt) was found to be the lowest energy conformer in the $G^{\pm}G^{\pm}G^{\pm}$(xyz) cluster, while the $G^{\pm}G^{\pm}T$ (ttt) structure was the lowest in energy corresponding to the $G^{\pm}G^{\pm}T$(xyz) cluster, with the $G^{\pm}G^{\pm}G^{\pm}$ (ttt) conformer being the global minimum. Furthermore, consistent with our predictive scheme, it can be seen that the energies of the conformers generally increased as we progressively increase the number of terminal carbon atoms adopting a *gauche* orientation. It may also be noted that due to the lower symmetry of $G^{\pm}G^{\pm}T$(xyz) structures, some of the conformational pairs, which were degenerate in the $G^{\pm}G^{\pm}G^{\pm}$(xyz) cluster, split in this case. For example, the $G^{\pm}G^{\pm}T(tg^{m}t)$ and $G^{\pm}G^{\pm}T(ttg^{m})$ are distinct conformers, while their counterparts in the $G^{\pm}G^{\pm}G^{\pm}$(xyz) cluster, the $G^{\pm}G^{\pm}G^{\pm}(tg^{m}t)$ and $G^{\pm}G^{\pm}G^{\pm}(ttg^{m})$ structures are degenerate. Clearly, the splitting of degeneracy in the $G^{\pm}G^{\pm}T$ (xyz) cluster gives rise to a significantly larger number of distinct conformers than that obtained for the $G^{\pm}G^{\pm}G^{\pm}$(xyz) cluster.

For a given conformation, two degenerate pairs exist related by symmetry. For example, the $G^{\pm}G^{\pm}T(ttg^{m})$ structure consists of two degenerate conformers, $G^{+}G^{+}T(ttg^{-})$ and $G^{-}G^{-}T$ (ttg^{+}). In addition, this set also contains a threefold degeneracy, where the *trans*-oriented carbon can be moved to any one of the three locations, thus giving a total degeneracy of six. In addition to such symmetry-related degeneracies, we have also encountered accidental degeneracies, such as with the $G^{\pm}G^{\pm}T(g^{m}g^{\pm}g^{m})$ and $G^{\pm}G^{\pm}T(tg^{m}g^{m})$ pairs. That this pair constitutes only accidental degeneracy is confirmed by the fact that the two structures have different dipole moments and vibrational frequencies.

Table II gives the molecular parameters defining the structures of the $G^{\pm}G^{\pm}G^{\pm}$(ttt) and $G^{\pm}G^{\pm}T$(ttt) conformers, which are the minima in their respective clusters. Figure 1 displays the structures of these conformers. For all the other conformers, only the dihedral angles, which differentiate the various structures, are presented in Table III. This study constitutes the first detailed report on the conformers of TEP.

Table I
Relative energies[a] and dipole moments[b] of the 35 conformers of TEP, calculated at the B3LYP/6–31G level**

Structure	$G^{\pm}G^{\pm}G^{\pm}$ cluster		$G^{\pm}G^{\pm}T$ cluster	
	ΔE (kcal/mol)	Dipole moment (D)	ΔE (kcal/mol)	Dipole moment (D)
$G^{\pm}G^{\pm}G^{\pm}$(ttt)	0	1.10		
$G^{\pm}G^{\pm}G^{\pm}$(ttg$^{\pm}$)	0.23	1.04		
$G^{\pm}G^{\pm}G^{\pm}$(ttg$^{\mp}$)	0.48	0.79		
$G^{\pm}G^{\pm}G^{\pm}$(tg$^{\pm}$g$^{\pm}$)	0.61	0.99		
$G^{\pm}G^{\pm}G^{\pm}$(tg$^{\pm}$g$^{\mp}$)	0.79	0.79		
$G^{\pm}G^{\pm}$T(ttt)			0.96	3.74
$G^{\pm}G^{\pm}G^{\pm}$(tg$^{\mp}$g$^{\mp}$)	1.02	0.54		
$G^{\pm}G^{\pm}$T(tg$^{\pm}$t)			1.12	3.64
$G^{\pm}G^{\pm}G^{\pm}$(g$^{\pm}$g$^{\pm}$g$^{\pm}$)	1.14	0.90		
$G^{\pm}G^{\pm}G^{\pm}$(g$^{\pm}$g$^{\mp}$g$^{\mp}$)	1.15	0.75		
$G^{\pm}G^{\pm}$T(g$^{\mp}$tt)			1.23	3.56
$G^{\pm}G^{\pm}G^{\pm}$(g$^{\pm}$g$^{\mp}$g$^{\mp}$)	1.27	0.52		
$G^{\pm}G^{\pm}$T(tg$^{\mp}$t)			1.28	3.55
$G^{\pm}G^{\pm}$T(g$^{\pm}$tt)			1.41	3.51
$G^{\pm}G^{\pm}$T(g$^{\mp}$g$^{\pm}$t)			1.42	3.41
$G^{\pm}G^{\pm}G^{\pm}$(g$^{\mp}$g$^{\mp}$g$^{\mp}$)	1.49	0.22		
$G^{\pm}G^{\pm}$T(ttg$^{\mp}$)			1.50	3.85
$G^{\pm}G^{\pm}$T(g$^{\pm}$g$^{\pm}$t)			1.59	3.59
$G^{\pm}G^{\pm}$T(tg$^{\pm}$g$^{\mp}$)			1.60	3.71
$G^{\pm}G^{\pm}$T(g$^{\mp}$g$^{\mp}$t)			1.62	3.32
$G^{\pm}G^{\pm}$T(g$^{\mp}$tg$^{\mp}$)			1.79	3.65
$G^{\pm}G^{\pm}$T(ttg$^{\pm}$)			1.81	3.92
$G^{\pm}G^{\pm}$T(g$^{\pm}$g$^{\mp}$t)			1.82	3.39
$G^{\pm}G^{\pm}$T(g$^{\mp}$g$^{\pm}$g$^{\mp}$)			1.90	3.47
$G^{\pm}G^{\pm}$T(tg$^{\mp}$g$^{\mp}$)			1.90	3.66
$G^{\pm}G^{\pm}$T(g$^{\pm}$tg$^{\mp}$)			1.98	3.66
$G^{\pm}G^{\pm}$T(g$^{\mp}$tg$^{\pm}$)			2.11	3.73
$G^{\pm}G^{\pm}$T(tg$^{\mp}$g$^{\pm}$)			2.19	3.74
$G^{\pm}G^{\pm}$T(g$^{\mp}$g$^{\mp}$g$^{\mp}$)			2.22	3.39
$G^{\pm}G^{\pm}$T(tg$^{\pm}$g$^{\pm}$)			2.35	3.68
$G^{\pm}G^{\pm}$T(g$^{\pm}$g$^{\mp}$g$^{\mp}$)			2.40	3.54
$G^{\pm}G^{\pm}$T(g$^{\mp}$g$^{\mp}$g$^{\mp}$)			2.40	3.49
$G^{\pm}G^{\pm}$T(g$^{\pm}$tg$^{\pm}$)			2.45	3.77
$G^{\pm}G^{\pm}$T(g$^{\mp}$g$^{\pm}$g$^{\pm}$)			2.64	3.50
$G^{\pm}G^{\pm}$T(g$^{\pm}$g$^{\pm}$g$^{\pm}$)			2.97	3.60

[a]Energies are relative to the $G^{\pm}G^{\pm}G^{\pm}$(ttt) conformer. All energies have been corrected for zero-point energy.

3.2. *Vibrational assignments*

Based on the energies of the various conformers and their degeneracies, the relative populations of the conformers at room temperature were calculated (Table IV). It can be seen that the population integrated over all the conformers corresponding to the $G^{\pm}G^{\pm}G^{\pm}$(xyz) cluster works out to about 63% of the total population, while those integrated over the conformers of the $G^{\pm}G^{\pm}$T(xyz) cluster works out to 37%. Since this room temperature population distri-

bution is likely to be trapped in the matrix, vibrational features of the conformers corresponding to both the clusters can be expected to be observed in the spectra of matrix-isolated TEP.

Tables V and VI give the computed vibrational frequencies of the first four conformers corresponding the $G^{\pm}G^{\pm}G^{\pm}$(xyz) and $G^{\pm}G^{\pm}T$(xyz) clusters, respectively. It can be seen that P = O stretching frequency for the two clusters of conformers differs significantly, allowing for the resolution of the conformers belonging to the two clusters. Similarly, there are differences in the P–(O–C) stretching modes that will allow for distinguishing the conformers between the two sets.

To bring the computed frequencies in agreement with the experimental results, we have used mode-by-mode scaling as reported for TMP [2]. We resorted to this scaling as the matrix perturbations may be different for different modes and this procedure at least empiri-

Table II
Selected structural parameters[a] of the $G^{\pm}G^{\pm}G^{\pm}$(ttt) and $G^{\pm}G^{\pm}T$(ttt) conformers of TEP computed at the B3LYP/6–31G level**

Parameter	$G^{\pm}G^{\pm}G^{\pm}$(ttt)	$G^{\pm}G^{\pm}T$(ttt)
P^1–O^2	1.482	1.476
P^1–O^3	1.607	1.608
P^1–O^4	1.607	1.621
P^1–O^5	1.607	1.602
C^6–O^3	1.450	1.450
C^7–O^4	1.450	1.451
C^8–O^5	1.450	1.449
C^9–C^6	1.516	1.516
C^{12}–C^7	1.516	1.516
C^{15}–C^8	1.516	1.516
O^3–P^1–O^2	116.3	118.1
O^4–P^1–O^2	116.2	115.0
O^5–P^1–O^2	116.3	113.4
C^6–O^3–P^1	118.9	119.0
C^7–O^4–P^1	119.0	118.7
C^8–O^5–P^1	119.0	121.7
C^9–C^6–O^3	107.9	108.0
C^{12}–C^7–O^4	107.9	107.9
C^{15}–C^8–O^5	107.9	107.8
$O^4P^1O^2O^3$	119.9	118.8
$O^5P^1O^2O^3$	–120.0	–118.7
$C^6O^3P^1O^2$	45.0	51.9
$C^7O^4P^1O^2$	44.9	36.0
$C^8O^5P^1O^2$	44.9	177.4
C^9C^6–O^3P^1	189.4	187.8
$C^{12}C^7O^4P^1$	190.0	190.5
$C^{15}C^8O^5P^1$	189.5	173.1

[a]Bond lengths are in Å and bond angles and dihedral angles are in degrees.

Table III
Selected dihedral angles (°) of the 33 other conformers of TEP computed at the B3LYP/6–31G level**

Structure	$C^6O^3P^1O^2$	$C^7O^4P^1O^2$	$C^8O^5P^1O^2$	$C^9C^6O^3P^1$	$C^{12}C^7O^4P^1$	$C^{15}C^8O^5P^1$
$G^{\pm}G^{\pm}G^{\pm}(ttg^{\pm})$	50.1	46.6	34.2	190.0	188.9	91.6
$G^{\pm}G^{\pm}G^{\pm}(ttg^{\mp})$	44.5	45.4	40.8	192.5	191.4	–90.0
$G^{\pm}G^{\pm}G^{\pm}(tg^{\pm}g^{\pm})$	51.6	38.0	37.6	186.0	92.9	92.2
$G^{\pm}G^{\pm}G^{\pm}(tg^{\pm}g^{\mp})$	46.2	34.8	49.3	190.6	93.3	–88.7
$G^{\pm}G^{\pm}G^{\pm}(tg^{\mp}g^{\mp})$	45.0	43.4	41.3	190.9	–90.0	–89.7
$G^{\pm}G^{\pm}G^{\pm}(g^{\pm}g^{\pm}g^{\pm})$	40.9	40.9	40.5	92.8	93.9	92.8
$G^{\pm}G^{\pm}G^{\pm}(g^{\pm}g^{\mp}g^{\pm})$	39.3	52.9	35.8	92.6	–86.9	91.5
$G^{\pm}G^{\pm}G^{\pm}(g^{\pm}g^{\mp}g^{\mp})$	35.3	51.4	38.9	93.5	–87.3	–94.0
$G^{\pm}G^{\pm}G^{\pm}(g^{\mp}g^{\mp}g^{\mp})$	41.4	41.8	41.6	–90.9	–90.8	–91.0
$G^{\pm}G^{\pm}T(tg^{\pm}t)$	56.2	28.5	178.4	187.0	84.1	173.7
$G^{\pm}G^{\pm}T(g^{\mp}tt)$	53.8	34.3	178.4	–86.0	191.6	172.0
$G^{\pm}G^{\pm}T(tg^{\mp}t)$	53.5	29.6	180.2	186.5	–93.5	173.7
$G^{\pm}G^{\pm}T(g^{\pm}tt)$	38.3	40.1	176.8	95.1	188.5	174.4
$G^{\pm}G^{\pm}T(g^{\mp}g^{\pm}t)$	56.1	27.7	179.1	–85.6	85.0	175.2
$G^{\pm}G^{\pm}T(ttg^{\mp})$	54.2	38.3	178.9	190.2	191.1	–103.1
$G^{\pm}G^{\pm}T(g^{\pm}g^{\pm}t)$	49.5	31.2	177.3	102.5	86.6	175.1
$G^{\pm}G^{\pm}T(tg^{\pm}g^{\mp})$	56.4	30.6	179.1	186.8	84.0	–104.2
$G^{\pm}G^{\pm}T(g^{\mp}g^{\mp}t)$	53.8	31.2	179.8	–85.3	–91.6	173.8
$G^{\pm}G^{\pm}T(g^{\mp}tg^{\mp})$	55.8	36.8	178.3	–85.4	193.9	–104.1
$G^{\pm}G^{\pm}T(ttg^{\pm})$	55.3	31.6	177.8	187.9	196.9	98.8
$G^{\pm}G^{\pm}T(g^{\pm}g^{\mp}t)$	42.9	39.3	178.4	98.8	–90.1	174.7
$G^{\pm}G^{\pm}T(g^{\mp}g^{\pm}g^{\mp})$	56.7	30.9	177.9	–85.3	84.8	–105.3
$G^{\pm}G^{\pm}T(tg^{\mp}g^{\mp})$	55.0	33.8	181.1	186.7	–93.4	–102.2
$G^{\pm}G^{\pm}T(g^{\pm}tg^{\mp})$	41.6	41.8	178.4	97.1	184.9	–102.5
$G^{\pm}G^{\pm}T(g^{\mp}tg^{\mp})$	56.9	32.2	176.8	–84.5	196.6	97.2
$G^{\pm}G^{\pm}T(tg^{\mp}g^{\pm})$	56.6	29.5	177.9	187.3	–93.5	97.6
$G^{\pm}G^{\pm}T(g^{\mp}g^{\mp}g^{\mp})$	54.3	34.1	180.6	–85.7	–90.9	–103.4
$G^{\pm}G^{\pm}T(tg^{\pm}g^{\pm})$	57.1	24.7	166.7	187.0	84.2	88.5
$G^{\pm}G^{\pm}T(g^{\pm}g^{\mp}g^{\mp})$	46.9	39.5	179.6	100.8	–90.6	–103.3
$G^{\pm}G^{\pm}T(g^{\mp}g^{\mp}g^{\pm})$	55.5	28.7	181.4	–86.3	–91.7	106.9
$G^{\pm}G^{\pm}T(g^{\pm}tg^{\pm})$	45.3	37.1	174.0	100.1	194.5	96.9
$G^{\pm}G^{\pm}T(g^{\mp}g^{\pm}g^{\pm})$	59.3	23.0	166.9	–82.9	83.0	85.4
$G^{\pm}G^{\pm}T(g^{\pm}g^{\pm}g^{\pm})$	50.5	25.0	166.7	102.0	82.4	89.1

cally corrects for this systematic variation. We have restricted our discussion to the modes involving the P = O, CH_2, P–(O–C), (P–O)–C, and C–C vibrations as these are the modes that have the largest infrared intensities in the TEP spectra.

3.2.1. *P = O Vibration*

Vidya *et al*. assigned the feature at 1270.5 cm^{-1} to the P = O stretch of the ground state conformer (*G*) of TEP, and the 1305.2 cm^{-1} to the same mode in higher energy conformer(s) (*H*) (Fig. 2(a)) [5]. This assignment implies that the 1270.5 cm^{-1} feature must be, significantly, due to the $G^{\pm}G^{\pm}G^{\pm}$(ttt) conformer which has been computed to be global minimum on the TEP conformation potential surface. The computed feature for this conformer was 1283.3 cm^{-1}, which implies a scaling factor of 0.990. This factor was then used to scale the

computed P = O frequencies for all the other conformers in both the $G^{\pm}G^{\pm}G^{\pm}$(xyz) and $G^{\pm}G^{\pm}T$(xyz) clusters. It can be seen that the P = O stretching frequency for the conformers in the $G^{\pm}G^{\pm}G^{\pm}$(xyz) clusters occur near 1270 cm^{-1}. Furthermore, at least four of the conformers in this cluster have populations near or in excess of 10% (Table IV), which implies that all of them may contribute to the 1270 feature. In fact, these four conformers in the $G^{\pm}G^{\pm}G^{\pm}$(xyz) cluster together contribute to more than 40% of the total population. It must also be noted that the first three higher energy conformers, $G^{\pm}G^{\pm}G^{\pm}(ttg^{\pm})$, $G^{\pm}G^{\pm}G^{\pm}(ttg^{m})$, and $G^{\pm}G^{\pm}G^{\pm}(tg^{\pm}g^{\pm})$, with an energy, 0.23. 0.48 and 0.61 kcal/mol, respectively, higher than the global minimum, contribute more to the overall population than the global minimum, due to

Table IV
Energies (kcal/mol), degeneracies and populations of the various conformers of TEP

Structure	Energy	Degeneracy	Population (% of the total)
$G^{\pm}G^{\pm}G^{\pm}(ttt)$	0	2	8.1
$G^{\pm}G^{\pm}G^{\pm}(ttg^{\pm})$	0.23	6	16.4
$G^{\pm}G^{\pm}G^{\pm}(ttg^{m})$	0.48	6	10.9
$G^{\pm}G^{\pm}G^{\pm}(tg^{\pm}g^{\pm})$	0.61	6	8.8
$G^{\pm}G^{\pm}G^{\pm}(tg^{\pm}g^{m})$	0.79	6	6.4
$G^{\pm}G^{\pm}G^{\pm}(tg^{m}g^{m})$	1.02	6	4.4
$G^{\pm}G^{\pm}G^{\pm}(g^{\pm}g^{\pm}g^{\pm})$	1.14	2	1.2
$G^{\pm}G^{\pm}G^{\pm}(g^{\pm}g^{m}g^{\pm})$	1.15	6	3.6
$G^{\pm}G^{\pm}G^{\pm}(g^{\pm}g^{m}g^{m})$	1.27	6	2.9
$G^{\pm}G^{\pm}G^{\pm}(g^{m}g^{m}g^{m})$	1.49	2	0.7
$G^{\pm}G^{\pm}T(ttt)$	0.96	6	4.9
$G^{\pm}G^{\pm}T(tg^{\pm}t)$	1.12	6	3.7
$G^{\pm}G^{\pm}T(g^{m}tt)$	1.23	6	3.1
$G^{\pm}G^{\pm}T(tg^{m}t)$	1.28	6	2.9
$G^{\pm}G^{\pm}T(g^{\pm}tt)$	1.41	6	2.3
$G^{\pm}G^{\pm}T(g^{m}g^{\pm}t)$	1.42	6	2.3
$G^{\pm}G^{\pm}T(ttg^{m})$	1.50	6	2.0
$G^{\pm}G^{\pm}T(g^{\pm}g^{\pm}t)$	1.59	6	1.7
$G^{\pm}G^{\pm}T(tg^{\pm}g^{m})$	1.60	6	1.7
$G^{\pm}G^{\pm}T(g^{m}g^{m}t)$	1.62	6	1.6
$G^{\pm}G^{\pm}T(g^{m}tg^{m})$	1.79	6	1.2
$G^{\pm}G^{\pm}T(ttg^{\pm})$	1.81	6	1.2
$G^{\pm}G^{\pm}T(g^{\pm}g^{m}t)$	1.82	6	1.1
$G^{\pm}G^{\pm}T(g^{m}g^{\pm}g^{m})$	1.90	6	1.0
$G^{\pm}G^{\pm}T(tg^{m}g^{m})$	1.90	6	1.0
$G^{\pm}G^{\pm}T(g^{\pm}tg^{m})$	1.98	6	0.9
$G^{\pm}G^{\pm}T(g^{m}tg^{\pm})$	2.11	6	0.7
$G^{\pm}G^{\pm}T(tg^{m}g^{\pm})$	2.19	6	0.6
$G^{\pm}G^{\pm}T(g^{m}g^{m}g^{m})$	2.22	6	0.6
$G^{\pm}G^{\pm}T(tg^{\pm}g^{\pm})$	2.35	6	0.5
$G^{\pm}G^{\pm}T(g^{\pm}g^{m}g^{m})$	2.40	6	0.4
$G^{\pm}G^{\pm}T(g^{m}g^{m}g^{\pm})$	2.40	6	0.4
$G^{\pm}G^{\pm}T(g^{\pm}tg^{\pm})$	2.45	6	0.4
$G^{\pm}G^{\pm}T(g^{m}g^{\pm}g^{\pm})$	2.64	6	0.3
$G^{\pm}G^{\pm}T(g^{\pm}g^{\pm}g^{\pm})$	2.97	6	0.2

Table V
Scaled computed frequencies (B3LYP/6–31G), experimental vibrational frequencies of the $G^{\pm}G^{\pm}G^{\pm}$(xyz) cluster of conformers of TEP and scaling factors**

Mode	$G^{\pm}G^{\pm}G^{\pm}$(ttt)	$G^{\pm}G^{\pm}G^{\pm}$(ttg$^{\pm}$)	$G^{\pm}G^{\pm}G^{\pm}$(ttg$^{\mp}$)	$G^{\pm}G^{\pm}G^{\pm}$(tg$^{\pm}$g$^{\pm}$)	Expt. (MI)	Scaling factor
P = O	1270.5 (157) [a]	1266.7 (161)	1266.1 (154)	1265.1 (166)	1270.5 1305.2	0.990
CH_2	1290.5 (16)	1286.9 (7)	1287.2 (7)	1289.9 (3)	1290.0 1293.5 1273.4	0.984
P–(O–C)	1042.5 (468) 1043.2 (473)	1036.6 (421) 1041.6 (471)	1037.1 (423) 1041.7 (465)	1035.6 (417) 1040.2 (455)	1047.1 1042.5 1050.4 1033.7	0.981
(P–O)–C + CH_2 +CH_3	991.0 (271) 988.0 (266)	988.4 (178) 978.0 (270)	990.6 (171) 977.2 (274)	984.0 (225) 964.1 (201)	991.0 988.3 976.4	1.01
(P–O)–C + CH_3	826.5 (30) 820.7 (33) 759.1 (31)	826.6 (42) 808.8 (46) 745.3 (38)	826.4 (33) 804.1 (45) 746.4 (34)	815.7 (51) 801.6 (57) 733.7 (41)	826.5 820.7 811.9	1.00

[a] Vibrational frequencies are in cm^{-1}.
The computed intensities (km/mol) for each mode are given in parenthesis.

a larger degeneracy, and are likely, therefore, to be significant contributors to the intensity of the 1270 feature. However, all these conformers have vibrational frequencies too closely spaced to be individually resolved. Table V gives the scaled computed frequencies of the four conformers mentioned above (which are the major contributors to the infrared intensities in this cluster of conformers), together with our experimentally observed frequencies.

The computed frequencies for the same mode in the conformers corresponding to the $G^{\pm}G^{\pm}T$(xyz) cluster occur near 1305 cm^{-1} and can therefore be clearly resolved from the $G^{\pm}G^{\pm}G^{\pm}$(xyz) cluster of conformers. Here again, a few conformers are likely to contribute to the 1305 feature, with the lowest energy form in this cluster, $G^{\pm}G^{\pm}T$(ttt) being the major contributor. Table VI gives the scaled computed frequencies of the four dominant conformers in the $G^{\pm}G^{\pm}T$(xyz) cluster, together with our experimentally observed frequencies.

The assignments of Vidya *et al*. can therefore be rationalized as follows: the 1270 cm^{-1} feature assigned to conformer *G* must be correlated to the $G^{\pm}G^{\pm}G^{\pm}$(xyz) cluster of conformers, while the 1305 cm^{-1} feature assigned to conformer *H* must be correlated to the $G^{\pm}G^{\pm}T$(xyz) cluster of conformers.

Trace 2a in Fig. 2 was obtained using an effusive source and therefore represents a population distribution corresponding to room temperature. Trace 2b was obtained using a supersonic source, where the cooling in the expansion is expected to deplete the higher energy conformers. It is clear from this trace that the 1305 feature, assigned to the higher energy $G^{\pm}G^{\pm}T$(xyz) cluster, disappears. Furthermore, the 1270 feature assigned to the $G^{\pm}G^{\pm}G^{\pm}$(xyz) cluster of conformers also sharpens in the spectra recorded using a supersonic

Table VI
Scaled computed frequencies (B3LYP/6–31G), experimental vibrational frequencies of the $G^{\pm}G^{\pm}T$(xyz) cluster of conformers of TEP and scaling factors**

Mode	$GG^{\pm}T$(ttt)	$G^{\pm}G^{\pm}T(tg^{\pm}t)$	$G^{\pm}G^{\pm}T$ ($g^{\mp}tt$)	$G^{\pm}G^{\pm}T(tg^{\mp}t)$	Expt (MI)	Scaling factor
P = O	1305.1(102)[a]	1299.3 (70)	1299.1 (44)	1299.8 (67)	1270.5 1305.2	0.990
CH_2	1277.2 (117)	1280.6 (148)	1277.1 (142)	1281.0 (144)	1290.0 1293.5 1273.4	0.984
P–(O–C)	1039.7 (371) 1048.8 (433)	1038.9 (365) 1048.0 (407)	1036.9 (370) 1048.3 (433)	1035.4 (308) 1050.0 (481)	1047.1 1042.5 1050.4 1033.7	0.981
(P–O)–C + CH_2 + CH_3	990.7 (218) 976.0 (201)	989.9 (159) 976.4 (188) 942.3 (112)	988.0 (159) 969.7 (188) 950.9 (78)	991.2 (204) 976.5 (109) 938.4 (115)	991.0 988.3 976.4	1.01
(P–O)–C + CH_3	830.5 (72) 814.2 (85) 739.6 (11)	822.0 (26) 819.4 (28) 807.1 (90)	828.8 (80) 796.8 (86)	828.1 (57) 803.6 (84)	826.5 820.7 811.9	1.00

[a]Vibrational frequencies are in cm^{-1}.
The computed intensities (km/mol) for each mode are given in parenthesis.

beam. This observation indicates that this feature received contributions from more than one conformer in the $G^{\pm}G^{\pm}G^{\pm}$(xyz) cluster, and the cooling in the beam had resulted, in some of the higher energy forms in the cluster, to be depleted. The experimental observations of Vidya *et al*. are therefore well explained by the conformational picture derived in this study.

3.2.2. *Vibrational mixing between P=O and CH_2 modes in $G^{\pm}G^{\pm}T$(ttt) conformer*

A doublet seen at 1290.0 and 1293.5 cm^{-1} was assigned in our earlier work to the CH_2 twisting mode of TEP (Fig. 2(a)). Our computed scaled frequencies for this mode agree well with the experimental features.

From Table V, it can be seen that the intensity of the P = O vibration in the $G^{\pm}G^{\pm}G^{\pm}$(ttt) and other conformers in this cluster is ~155 km/mol. However, the same feature in the $G^{\pm}G^{\pm}T$(ttt) conformer and others in this cluster (Table VI) is somewhat weaker in intensity (not exceeding 100 km/mol). Correspondingly, the intensity of the CH_2 twisting, in the $G^{\pm}G^{\pm}G^{\pm}$(xyz) cluster, is ~15 km/mol, while it is significantly stronger in the $G^{\pm}G^{\pm}T$(xyz) cluster of conformers, with an intensity of ~120 km/mol.

An analysis of the normal modes using the GaussView program reveals a vibrational mixing between the P = O stretch and CH_2 twist in the $G^{\pm}G^{\pm}T$(ttt) conformer. As a result of this mixing, the intensity of the CH_2 mode gains at the expense of the intensity of the P=O vibration in the $G^{\pm}G^{\pm}T$(ttt) conformer. No such mode mixing is indicated in the $G^{\pm}G^{\pm}G^{\pm}$(xyz) cluster of conformers.

It must be mentioned that the sharpening of the 1270 feature in the spectrum recorded with the supersonic source may also have been contributed due to this phenomenon. The

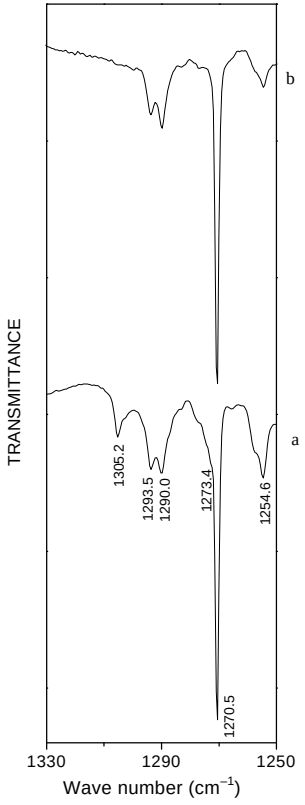

FIG. 2. Spectra of matrix-isolated TEP in the region of 1330–1250 cm^{-1} using (a) an effusive source, and (b) supersonic jet source at a stagnation pressure of 1000 torr.

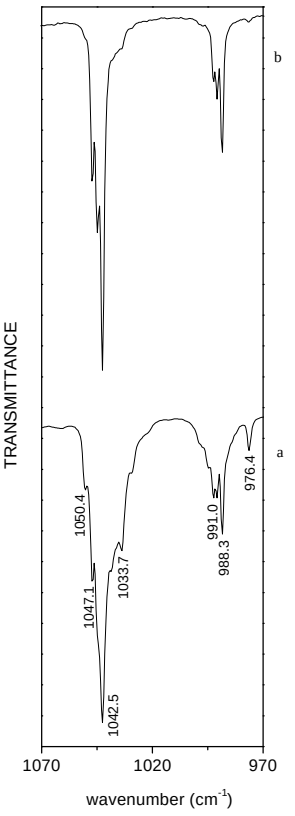

FIG. 3. Spectra of matrix-isolated TEP in the region of 1070–970 cm^{-1} using (a) an effusive source, and (b) supersonic jet source at a stagnation pressure of 1000 torr.

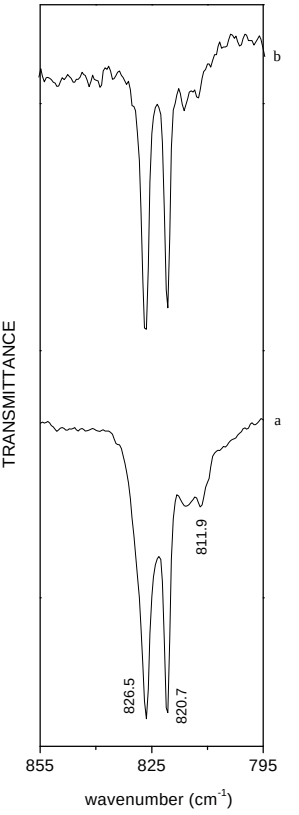

FIG. 4. Spectra of matrix-isolated TEP in the region of 855–795 cm^{-1} using (a) an effusive source, and (b) supersonic jet source at a stagnation pressure of 1000 torr.

mixed P = O/CH_2 twisting mode for the $G^{\pm}G^{\pm}T$(xyz) cluster has a component near 1270 cm^{-1} and probably overlaps with the pure P = O mode of the $G^{\pm}G^{\pm}G^{\pm}$(xyz) clusters and contributes to the intensity of the 1270 feature. In the supersonic beam, the higher energy $G^{\pm}G^{\pm}T$ (xyz) cluster is depleted and hence this contribution is lost, which results in the sharpening of this feature.

In order to confirm that the vibrational mixing was responsible for the intensity changes seen in the $G^{\pm}G^{\pm}T$(ttt) conformer of TEP, computations were done for the $G^{\pm}G^{\pm}T$(ttt) conformer of TEP, where all the hydrogens in the three methylene groups were substituted by deuterium. The mode involving CD_2 occurs near 900 cm^{-1}, which is well removed from the P = O mode of the $G^{\pm}G^{\pm}T$(ttt) conformer; consequently, vibrational mixing is suppressed in this molecule, as indicated by the computations. The P = O feature of the $G^{\pm}G^{\pm}T$(ttt) conformer in the deuterated TEP has an intensity of ~ 200 km/mole and the CD_2 twisting mode ~ 6 km/mole, in line with the intensities of the $G^{\pm}G^{\pm}G^{\pm}$(xyz) cluster of conformers, where

no vibrational mixing was observed. Due to the nonavailability of the deuterated compound, experiments could not be performed using deuterated TEP.

3.2.3. *P-(O-C) Vibration*

Vidya *et al*. assigned the 1042.5 cm^{-1} along with the satellite features at 1047.1 and 1044.9 cm^{-1} to the ground state conformer (*G*), while the significantly depopulated 1033.7 cm^{-1} features in the supersonic expansion were assigned to higher energy conformer(s) (*H*) (Fig. 3). The raw computed frequency for this mode in the $G^{\pm}G^{\pm}G^{\pm}$(ttt) form appears as two nearly degenerate modes at ~ 1062 cm^{-1} (Table V). We therefore assign this feature to the ground state conformer, which implies a scaling factor of 0.981. The scaled computed frequencies for the other forms in the $G^{\pm}G^{\pm}G^{\pm}$(xyz) cluster occur at frequencies that are close to the experimental values of 1042.5 and 1047.1 cm^{-1}. The computed frequencies for the $G^{\pm}G^{\pm}$T(ttt) conformer occur at 1039.7 and 1048.8 cm^{-1} (Table VI). The other conformers in this cluster also have frequencies for this mode near these values. The supersonic beam expansion experiments show a clear sharpening of the 1042.5 cm^{-1} feature, particularly in the regions near 1033 and 1050 cm^{-1}, where the higher energy conformers are computed to contribute, thus corroborating the assignment of the features for the various conformers.

3.2.4. *(P-O)-C and C–C Vibrations*

These two modes appear to be mixed in TEP and hence it is not possible to assign the features individually to these modes. Vidya *et al*. assigned the 988.3 cm^{-1} along with the satellite feature 991.0 cm^{-1} to the ground state conformer (*G*), while the significantly depopulated 976.4 cm^{-1} feature in the supersonic expansion was assigned to the higher energy conformer(s) (*H*) (Fig. 3). Our computations indicate that while the 988 cm^{-1} feature receives contributions both from the ground and excited state conformers, the 976 cm^{-1} feature receives significant contributions only from the higher energy conformers and hence its reduction in intensity in the supersonic beam experiment stands corroborated.

Vidya *et al*. assigned the doublet near 820 cm^{-1} (820.7 and 826.5 cm^{-1}) to the ground and higher energy conformer. It was argued that for this mode, both the *G* and *H* conformers could be having unresolved features. This observation is consistent with our computation, which indicates that the 820 and the 826 cm^{-1} features received significant contributions from both ground and higher energy conformers (Table VI and Fig. 4).

4. Dipole moments

The reported experimental dipole moment of TEP in benzene solution was 3.07 D at 298 K [15]. The B3LYP/6–31G** computed dipole moments of the various conformers of TEP are shown in Table I. Using the computed dipole moments for each conformer and its relative population, the dipole moment of TEP averaged over the different conformers was calculated. The overall dipole moment of TEP thus calculated is 2.3 D, which, considering the complex conformational picture for this molecule, is reasonably close to the experimental value of 3.07 D. It may also be noted that in TMP the $G^{\pm}G^{\pm}G^{\pm}$ conformer had the lower dipole moment compared with the $G^{\pm}G^{\pm}$T conformer. In TEP, the cluster of conformers correlating with this structure of TMP, i.e. the $G^{\pm}G^{\pm}G^{\pm}$(xyz) cluster of conformers, all had dipole moments that are smaller than the dipole moments of the $G^{\pm}G^{\pm}$T(xyz) cluster.

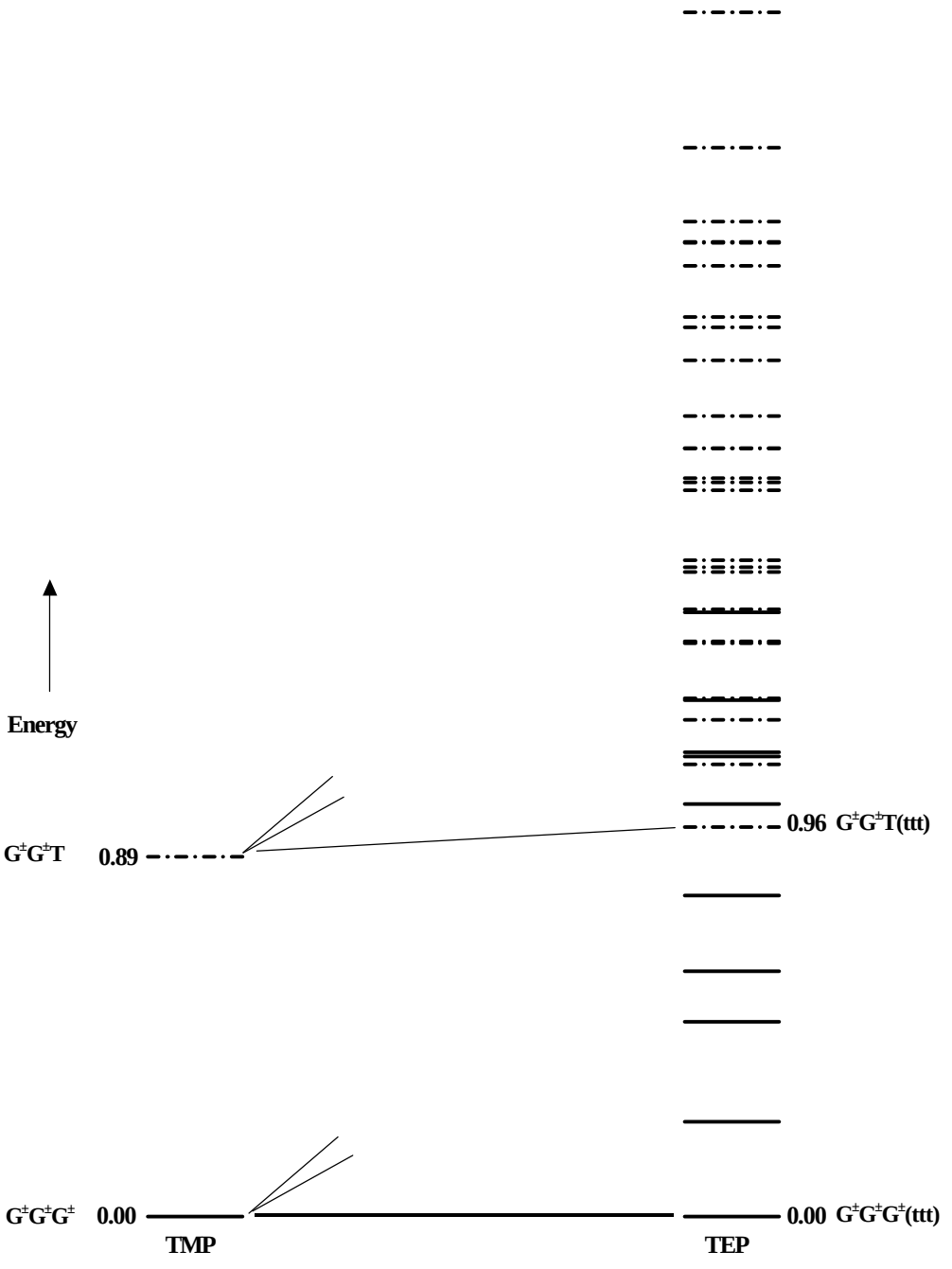

FIG. 5. Diagram showing the correlation between the conformers in TMP and TEP. The solid lines refer to conformers in the GGG clusters while the broken lines refer to the GGT cluster of conformers.

5. Comparison of the conformations in TMP and TEP

A correlation diagram can be drawn between the conformations of the TMP and TEP. As discussed earlier, the $G^{\pm}G^{\pm}G^{\pm}$ and $G^{\pm}G^{\pm}G^{\pm}$(ttt) conformers were the ground states in TMP and TEP, respectively. Interestingly, the energy difference, at the B3LYP/6-31G** level, between the two conformers of TMP, $G^{\pm}G^{\pm}G^{\pm}$ and $G^{\pm}G^{\pm}T$ (0.89 kcal/mol) is close to the energy difference between the lowest energy conformers correlating with these states, i.e. $G^{\pm}G^{\pm}G^{\pm}$(ttt) and $G^{\pm}G^{\pm}T$(ttt) conformer in TEP (0.96 kcal/mol) (Fig. 5). This result is similar to our earlier observation regarding the correlation of conformational patterns in DMM and DEM [11].

We also examined if any intramolecular hydrogen bonding interactions were involved in stabilizing any of the conformers in TEP. An examination of the charge-density topology of all the conformers of TEP, using the atoms-in-molecule (AIM) theory of Bader [16], showed that a (3, –1) bond critical point associated with an intramolecular C–H···O (alkoxy oxygen) interaction could be identified *only* for the $G^{\pm}G^{\pm}G^{\pm}(g^{\pm}g^{\pm}g^{\pm})$ conformer. However, this conformer does not contribute significantly at room temperatures, and therefore it must be concluded that at least for the conformers that contribute to the chemistry of TEP at room temperature, intramolecular hydrogen bonding interactions do not play a role.

In a number of structures, including the $G^{\pm}G^{\pm}G^{\pm}$(ttt) and $G^{\pm}G^{\pm}T$(ttt) conformers, the distance between one of the methylene hydrogens and the phosphoryl oxygen was ~2.6 Å which is a reasonable C–H···O contact for a hydrogen bond. However, the electron-density analysis using AIM does not indicate a bond critical point in these conformers corresponding to the intramolecular hydrogen bond, thus excluding the possibility of such hydrogen bonds playing a role in determining conformational preferences in this system. In our earlier work, using the AM1 analysis, we had indicated the possibility of such H-bonds playing a role, simply based on the distances of the C–H···O contacts [5]. This work clearly indicates that distances of C–H···O contacts do not serve as sufficient conditions for the formation of H-bonds; it must be complemented with investigations to identify the bond critical points.

6. Conclusions

This work together with the matrix isolation work reported earlier has led to a clear understanding of the spectra and structure of TEP. Our predictive scheme greatly simplified our search for the conformers of TEP. The ground state conformer of TEP was computed to be the $G^{\pm}G^{\pm}G^{\pm}$(ttt) form, where the anomeric carbons adopt a *gauche* orientation, while the terminal carbons have a *trans* orientiation. A number of conformers in the $G^{\pm}G^{\pm}G^{\pm}$(xyz) cluster, in addition to the $G^{\pm}G^{\pm}G^{\pm}$(ttt) form, were also found to contribute to the population at room temperature. In addition, our experiments also clearly showed the presence of conformers of TEP correlating with the $G^{\pm}G^{\pm}T$ form of TMP, with the $G^{\pm}G^{\pm}T$(ttt) struture being the lowest in energy in this cluster. Here too, in addition to the $G^{\pm}G^{\pm}T$(ttt) form, a number of conformers in the $G^{\pm}G^{\pm}T$(xyz) cluster contributed to the room temperature conformational population of TEP.

Excellent agreement was found between our computed values and the experimental frequencies reported by Vidya *et al*. This work has led to definitive assignment of the various infrared features of TEP.

Interestingly, our earlier work using AM1 computations, yielded many of the structures that were similar to those obtained by the present *ab initio* computations described in this work. In fact, the $G^{\pm}G^{\pm}G^{\pm}$(ttt) structure was one of the minima identified by the AM1 computations, but it did not indicate this struture to be global minimum. As mentioned in our earlier work, the energy ordering of the AM1 computations, turns out to be not so reliable.

This study has greatly facilitated the way we can predict and study the energy ordering of conformers in long-chain alkyl phosphates.

Acknowledgment

VV gratefully acknowledges the grant of a research fellowship from the Department of Atomic Energy, India, during the course of his work in this laboratory.

References and notes

1. V. Vidya, K. Sankaran, and K. S. Viswanathan, Matrix isolation–supersonic jet infrared spectroscopy: Conformational cooling in trimethyl phosphate, *Chem. Phys. Lett.*, **258**, 113–117 (1996).
2. L. George, K. S. Viswanathan, and S. J. Singh, *Ab initio* study of trimethyl phosphate: Conformational analysis, dipole moments, vibrational frequencies and barriers for conformer interconversion, *J. Phys. Chem. A*, **101**, 2459–2464 (1997).
3. R. Streck, A. J. Barnes, W. A. Herrebout, and B. J. van der Veken, Conformational behaviour of trimethyl phosphate studied by infrared spectroscopy, *J. Mol. Struct.*, **376**, 277–287 (1996).
4. I. Reva, A. Simao, and R. Fausto, Conformational properties of trimethyl phosphate monomer, *Chem. Phys. Lett.*, **406** 126–136 (2005).
5. V. Vidya, K. Sankaran, and K. S. Viswanathan, Conformations of triethyl phosphate: a supersonic jet–matrix isolation and semi-empirical (AM1) study, *J. Mol. Struct.*, **476**, 97–104 (1999).
6. V. Vidya, *Matrix isolation infrared spectroscopy of organic phosphates and some complexes: Utility of a supersonic jet source for such studies*, Ph. D. thesis, University of Madras (1997).
7. F. S. Mortimer, Vibrational assignment and rotational isomerism in some simple organic phosphates, *Spectrochim. Acta*, **9**, 270–281 (1957).
8. V. Venkatesan, K. Sundararajan, K. Sankaran, and K. S. Viswanathan, Conformations of dimethoxymethane: matrix isolation infrared and *ab initio* studies, S*pectrochim. Acta A*, **58**, 467–478 (2002).
9. V. Venkatesan, K. Sundararajan, and K. S. Viswanathan, Conformations of 1,1-dimethoxyethane: matrix isolation infrared and *ab Initio* studies, *J. Phys. Chem. A*, **106**, 7707–7713 (2002).
10. V. Venkatesan, K. Sundararajan, and K. S. Viswanathan, Matrix isolation infrared and *ab initio* study of the conformations of 2,2-dimethoxypropane, *Spectrochim. Acta A*, **59**, 1497–1507 (2003).
11. V. Venkatesan, K. Sundararajan, and K. S. Viswanathan, Conformations of diethoxymethane: matrix isolation infrared and *ab Initio* studies, *J. Phys. Chem. A*, **107**, 7727–7732 (2003).
12. In the C^{a}–O–C–O–C^{a} skeleton, the carbon atoms attached to the oxygen and labelled with a 'superscripted *a*' are the anomeric carbon atoms.
13. In the C^{t}–C^{a}–O–C^{a}–C^{t} skeleton, such as in DEM, the carbon atoms attached to the oxygen and labelled with a 'superscripted *a*' are the anomeric carbon atoms, while those labelled with a 'superscripted *t*' are the terminal carbon atoms.
14. M. J. Frisch, G. W. Trucks, H. B. Schlegel, G. E. Scuseria, M. A. Robb, J. R. Cheeseman, V. G. Zakrzewski, J. A. Montgomery Jr, R. E. Stratmann, J. C. Burant, S. Dapprich, J. M.Millam, A. D. Daniels, K. N. Kudin, M. C. Strain, O. Farkas, J. Tomasi, V. Barone, M. Cossi, R. Cammi, B. Mennucci, C. Pomelli, C. Adamo, S. Clifford, J. Ochterski, G. A. Petersson, P. Y. Ayala, Q. Cui, K. Morokuma, D. K. Malick, A. D. Rabuck, K.

Raghavachari, J. B. Foresman, J. Cioslowski, J. V. Ortiz, A. G. Baboul, B. B. Stefanov, G. Liu, A. Liashenko, P. Piskorz, I. Komaromi, R. Gomperts, R. L. Martin, D. J. Fox, T. Keith, M. A. Al-Laham, C. Y. Peng, A. Nanayakkara, M. Challacombe, P. M. W. Gill, B. Johnson, W. Chen, M. W. Wong, J. L. Andres, C. Gonzalez, M. Head-Gordon, E. S. Replogle, and J. A. Pople, *Gaussian 98*, Revision A.9, Gaussian Inc., Pittsburgh PA (1998).

15. L. McClellan, *Tables of experimental dipole moments*, W. H. Freeman, Vol. 1 (1963).
16. R. F. W. Bader, *Atoms in molecules*, Calendon Press (1994).